Hydroisomerization of *n*-Hexane Using Acidified Metal−Organic Framework and Platinum Nanoparticles

Kairat Sabyrov,[§,‡] Juncong Jiang,[†,§] Omar. M. Yaghi,*,[§,‖,⊥] and Gabor A. Somorjai*,[§,†,‖,‡]

§Department of Chemistry, ‖Kavli Energy NanoSciences Institute, University of California, Berkeley, Berkeley, California 94720, United States

‡Chemical and †Materials Sciences Division, Lawrence Berkeley National Laboratory, Berkeley, California 94720, United States

⊥King Abdulaziz City for Science and Technology, Post Office Box 6086, Riyadh 11442, Saudi Arabia

S *Supporting Information*

ABSTRACT: Exceptionally high surface area and ordered nanopores of a metal−organic framework (MOF) are exploited to encapsulate and homogeneously disperse a considerable amount of phosphotungstic acid (PTA). When combined with platinum nanoparticles positioned on the external surface of the MOF, the construct shows a high catalytic activity for hydroisomerization of *n*-hexane, a reaction requiring hydrogenation/dehydrogenation and moderate to strong Brønsted acid sites. Characterization of the catalytic activity and acidic sites as a function of PTA loading demonstrates that both the concentration and strength of acidic sites are highest for the catalyst with the largest amount of PTA. The MOF construct containing 60% PTA by weight produces isoalkanes with 100% selectivity and 9-fold increased mass activity as compared to a more traditional aluminosilicate catalyst, further demonstrating the capacity of the MOF to contain a high concentration of active sites necessary for the isomerization reaction.

Metal−organic frameworks (MOFs) are crystalline porous solids constructed from metal ion nodes linked in three dimensions by organic linkers.[1] MOFs have attracted much research attention because of their remarkable physical and chemical properties including but not limited to high surface area, tunable pore dimensions, adjustable chemical composition and surface functionality, and well-defined metal sites.[2] As a consequence, the performance of MOFs in some key gas storage and molecular separation applications is beginning to rival traditional microporous solids, such as zeolites and activated carbons.[3] Additionally, the number of reports on the use of MOFs in heterogeneous catalysis is increasing rapidly.[4] A select subset of such materials can be designed to contain coordinatively unsaturated metal sites that can serve as adsorption or catalytic sites for small molecules.[5] Another approach to designing a MOF based heterogeneous catalyst is to use MOF as a high surface area support or host for dispersing or encapsulating catalytically active species such as metal or metal oxide nanoclusters, organometallic complexes, and biological molecules or enzymes.[6]

In this work, we show that a MOF can serve as a bifunctional catalyst for *n*-hexane hydroisomerization, which requires moderate to strong acidic sites and hydrogenation/dehydrogen-

ation sites. The MOF (MIL-101) is "acidified" by encapsulating a large amount of phosphotungstic acid (PTA, $H_3PW_{12}O_{40}$) in the pores of the framework. Unlike with conventional mesoporous materials, complete dispersion of a significant amount of PTA (up to 60% by weight) is obtained with MIL-101 due to its exceptionally high surface area, ordered nanopores, and relatively high chemical stability. More importantly, well-defined platinum nanoparticles can be deposited on the external surface of the "acidified" MOF to obtain a highly active and selective bifunctional catalyst (PTA⊂MOF/Pt). At 250 °C and 1 bar, PTA⊂MOF/Pt catalyzes vapor-phase *n*-hexane isomerization with 100% selectivity and 9-fold increased mass activity as compared to a more traditional aluminosilicate bifunctional catalyst (Al-MCF-17/Pt).

Synthesis and Characterization of PTA⊂MIL-101. We synthesized PTA⊂MIL-101 by adding the necessary amount of PTA to a precursor mixture and crystallizing the MOF under hydrothermal conditions [see Supporting Information (SI), Section S1]. This method allowed us to uniformly disperse an extremely large amount of PTA without jeopardizing structural and compositional features of MIL-101 and the acid cluster. The primary reason for achieving high loading and high dispersion might be the formation of homogeneous mixture of PTA and the MOF precursors before crystallization. For more accurate characterization of the effect of PTA loading on the structure of the MOF, pure MIL-101 was compared to the MOF that contains 25% and 60% (by weight) PTA. Powder XRD patterns and TEM images of the samples are presented in Figure 1. Consistent with previous studies, pure MIL-101 particles were found to be octahedral in shape and possess highly crystalline and porous structure. Likewise, XRD patterns, TEM images, and N_2 physisorption studies of 25% and 60% PTA⊂MIL-101 are indicative of porous and crystalline structure of the samples. However, PTA containing MIL-101 crystals are highly aggregated and possess smaller and less uniform crystallite size than pure MIL-101 as shown in TEM (Figure 1b−d) and SEM (Figure S4) images. Scanning transmission electron microscopy (STEM) and elemental phase mapping of chromium (in MIL-101) and tungsten (in PTA) are also consistent with highly uniform distribution of
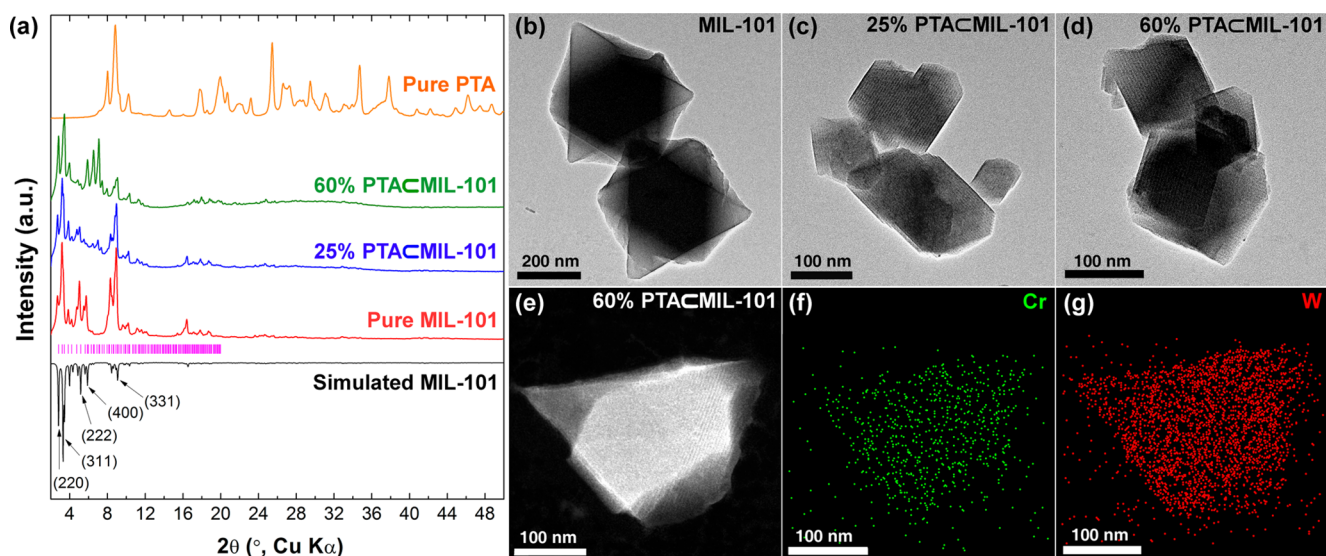
Figure 1. Powder XRD patterns for pure PTA, 60% PTA⊂MIL-101, 25% PTA⊂MIL-101, pure MIL-101 and simulated XRD pattern for pure MIL-101 (a). TEM images of pure MIL-101 (b) and MIL-101 that contains 25% (c) and 60% (d) phosphotungstic acid (PTA). Representative HDAAF-STEM image of 60% PTA⊂MIL-101 (e) and corresponding color-coded EDS spectral maps of chromium (Cr) in the framework of MIL-101 represented in green (f) and tungsten (W) in PTA cluster represented in red (g).

acid clusters within the MOF despite the markedly high mass loading. The lack of crystalline PTA domains detectable by powder XRD confirms that the acid cluster is indeed well dispersed throughout the structure and not only positioned on the external surface of the MOF. This is because the external surface area is less likely to accommodate such a high amount of PTA without forming crystalline structures. Previous studies on supported PTA showed that even the loading of the acid cluster on high surface area mesoporous silica with PTA amount as low as 20−30% (by weight) produces crystalline domains.[7] Furthermore, incorporation of PTA clusters in MIL-101 changed the porosity of the MOF as characterized by XRD and N_2 adsorption−desorption studies. With the loading of PTA in MIL-101, XRD pattern of the MOF underwent a noticeable change at low angles (4°−8°, Figure 1a). The degree of the change is highest for the sample that contains the largest amount of acid (60% PTA⊂MIL-101). These observations are in line with previous studies on PTA/MOF composite materials, suggesting the presence of ordered PTA assemblies residing in the pores of MIL-101. Consistent with XRD patterns, N_2 adsorption measurements clearly demonstrated the effect of PTA loading on the pore structure of the MOF. The incorporation of PTA not only changed the pore size distribution significantly but also decreased the accessible surface area of MIL-101 as presented in Figure S2. Finally, the samples were characterized by ^{31}P magic angle spinning nuclear magnetic resonance (^{31}P MAS NMR) and inductively coupled plasma atomic emission spectroscopy (ICP-AES) to ensure that the composition and Keggin structure of PTA in the MOF are intact. ^{31}P MAS NMR spectra of the both PTA containing MOF samples (25% and 60% PTA⊂MIL-101) showed a single peak at the same position as pure PTA (Figure S5), indicating that the Keggin structure of PTA was not altered during synthesis. In addition, elemental analysis by ICP-AES confirms that both 25% and 60% PTA⊂MIL-101 samples contain phosphorus (P) and tungsten (W) with the exact ratio of 1:12 as in the PTA Keggin cluster ($H_3PW_{12}O_{40}$).

***n*-Hexane Hydroisomerization.** In hydroisomerization of alkanes, acidic sites are coupled with metallic sites to produce

more efficient bifunctional catalysts.[8] Metals such as platinum and palladium activate alkanes to form dehydrogenated intermediate species, which then undergo protonation and isomerization at Brønsted acid sites.[9] In this work, platinum nanoparticles with well-defined particle size were synthesized using poly(vinylpyrrolidone) (PVP) as a capping agent and postsynthetically deposited on the external surface of PTA⊂MIL-101 (Figure S3). Isomerization of *n*-hexane was carried out at 250 °C and 1 bar on the MOF catalysts indicated as 60% PTA⊂MIL-101/Pt, 25% PTA⊂MIL-101/Pt, and MIL-101/Pt. As presented in Figure 2, the catalyst that contains the
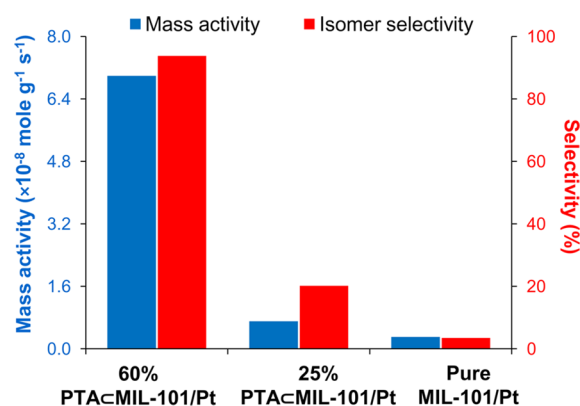
Figure 2. Total mass activity (blue) and isomer selectivity (red) of 60% and 25% PTA⊂MIL-101/Pt and MIL-101/Pt for hydro-isomerization of *n*-hexane in the gas phase at 250 °C and 1 bar.

highest amount of PTA was the most active and selective toward isoalkanes. However, the catalytic activity of 25% PTA⊂MIL-101/Pt and MIL-101/Pt was minimal.

The apparent difference in catalytic activity between PTA containing bifunctional catalysts indicates that the catalytic activity is not directly proportional to the amount of PTA cluster in the MOF. A similar phenomenon has been observed for PTA supported on mesoporous silica and metal oxides. It was demonstrated that HPAs possess strong acidic sites that

can react with surface oxides/hydroxides of silica and metal oxide supports, and lose some of their acidic character.[10] Similarly, upon loading of PTA in MIL-101, the acid might react with metal oxidic structural units of the MOF and lose a fraction of its acidic protons. Consequently, the catalyst with the lower amount of the acid (25% PTA⊂MIL-101/Pt) showed negligible catalytic activity indicating that most of its acidic protons were neutralized. In contrast, 60% PTA⊂MIL-101/Pt catalyzed *n*-hexane hydroisomerization with relatively high activity and selectivity as shown in Figure 2. This is presumably because the catalyst still contains a considerable amount of PTA with active Brønsted acid sites sufficient to isomerize *n*-hexane.

Characterization of Acidic Sites. On the basis of this hypothesis, we carried out qualitative characterization of acidic sites by adsorbing deuterated acetonitrile (CD$_3$CN) and taking infrared (IR) spectra of the catalysts. It is noteworthy to mention that so far no satisfactory technique exists for unambiguous characterization of acidic site strength and concentration for MOF based catalysts.[11] The conventional techniques such as pyridine adsorption/desorption and temperature-programmed ammonia desorption (NH$_3$-TPD) are not suitable for MOF catalysts due to the overlap of IR peaks of MOFs and probe molecules and limited thermal stability of MOFs. Here, we used CD$_3$CN as a probe molecule because it shows IR peaks in the clean region of the spectrum and the C≡N stretching absorption band has been shown to be highly sensitive to the interaction between the probe molecule and acid sites.[12] As presented in Figure 3, three bands
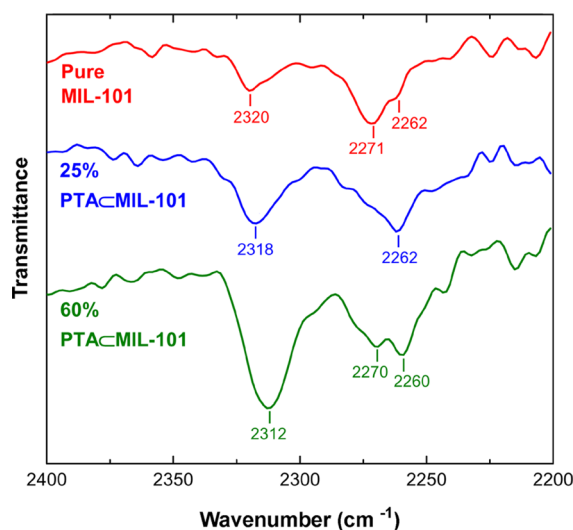
Figure 3. FTIR spectra of deuterated acetonitrile (CD$_3$CN) species adsorbed on pure MIL-101 and MIL-101 that contains 25% and 60% phosphotunstic acid (PTA).

of peaks were observed for the catalysts, one in the 2320−2312 cm^{-1} region, one at 2271−2270 cm^{-1}, and another at 2262−2260 cm^{-1}. The intensity of the IR peaks is quite low, making the quantitative characterization of acidic sites unrealistic. This is typical for CD$_3$CN presumably due to low basicity of the molecule. Nevertheless, on the basis of plentiful literature data on the characterization of zeolitic acid sites, the bands around 2271−2270 cm^{-1} and 2262−2260 cm^{-1} can be assigned to CD$_3$CN molecules adsorbed on nonacidic hydroxide groups (M—OH) and physisorbed CD$_3$CN, respectively.[13] The peak

at 2320 cm^{-1} observed for pure MIL-101 is consistent with adsorbed CD$_3$CN species on Lewis acid sites as previously determined for MIL-53 and zeolites.[13b,14] The additional adsorption bands at 2318 cm^{-1} and 2312 cm^{-1} observed for 25% and 60% PTA⊂MIL-101, respectively, are more likely due to protonated CD$_3$CN species at Brønsted acid sites. That is because PTA cluster contains only Brønsted acid sites in its structure. In addition, temperature dependent desorption studies on zeolites demonstrated that IR band around 2315 cm^{-1} corresponds to protonated species, acetonitrilium.[15]

The data on the characterization of acidic sites correspond well with the catalytic performance of the samples. The IR peak at 2312 cm^{-1} observed for 60% PTA⊂MIL-101 is noticeably higher in intensity than the peak at 2318 cm^{-1} observed for 25% PTA⊂MIL-101. Higher intensity of the peak suggests that the catalyst possesses higher concentration of Brønsted acid sites. Furthermore, the IR peak assigned for protonated CD$_3$CN species on 60% PTA⊂MIL-101 is observed at considerably lower wavenumbers than for the CD$_3$CN species on 25% PTA⊂MIL-101 (2312 vs 2318 cm^{-1}). The red-shift of the peak indicates the formation of stronger bonds between the probe molecule and the acidic sites. Accordingly, 60% PTA⊂MIL-101/Pt contains not only a larger number of acidic protons, but the strength of these acidic sites, necessary for the isomerization of dehydrogenated intermediate species, is substantially higher than the strength of the acidic sites of 25% PTA⊂MIL-101. All in all, the data indicate that both the concentration and strength of PTA clusters increase as a function of its incorporation in MIL-101.

PTA⊂MOF vs Aluminosilicate Catalyst. The performance of the catalytically active 60% PTA⊂MIL-101/Pt was evaluated against aluminosilicate catalyst previously studied for *n*-hexane hydroisomerization. Al-MCF-17/Pt was used as a reference bifunctional catalyst because of its high catalytic activity and remarkable selectivity toward hexane isomers.[8] As presented in Figure 4, both the MOF and aluminosilicate catalysts converted
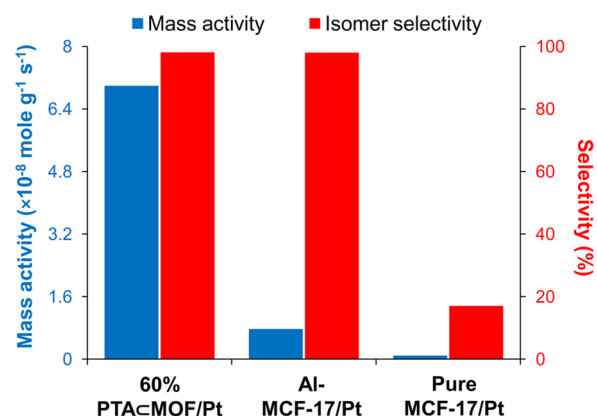
Figure 4. Mass activity (blue) and isomer selectivity (red) of the MOF based and aluminosilicate bifunctional catalysts and platinum nanoparticles supported onan inert mesoporous silica.

n-hexane with almost 100% isomer selectivity. Nevertheless, the mass activity of 60% PTA⊂MIL-101/Pt was significantly higher than the mass activity of Al-MCF-17/Pt and MCF-17/Pt. At 250 °C and 1 bar, 60% PTA⊂MIL-101/Pt showed 9-fold increased mass activity as compared to the aluminosilicate catalyst. The catalytic activity of MCF-17/Pt, which contains no acidic sites, was extremely low confirming the significance of

Brønsted acid sites for alkane isomerization. Finally, time-on-stream stability test of the MOF catalyst showed noticeable deactivation (Figure S8). Structural degradation might be contributing to the catalyst deactivation as revealed by XRD, N_2 uptake, and SEM characterization before and after the reaction (Figure S9). Nevertheless, the deactivation rate observed for the MOF catalyst is comparable to the deactivation of PTA supported on conventional oxides.[16] As such, common deactivating factors such as deposition of carbonaceous species or "coke" on active sites might also be contributing to the deactivation.

■ ASSOCIATED CONTENT

Ⓢ Supporting Information

The Supporting Information is available free of charge on the ACS Publications website at DOI: 10.1021/jacs.7b06629.

> Detailed description of materials synthesis, characterization, and catalytic studies, and figures illustrating N_2 adsorption measurements, TEM and SEM images, ^{31}P MAS NMR and FTIR spectra, TGA results in air and reducing atmosphere, and time-on-stream stability and characterization of the MOF catalyst before and after reaction (PDF)

■ AUTHOR INFORMATION

Corresponding Authors
*yaghi@berkeley.edu
*somorjai@berkeley.edu
ORCID
Omar. M. Yaghi: 0000-0002-5611-3325
Gabor A. Somorjai: 0000-0002-8478-2761
Notes
The authors declare no competing financial interest.

■ ACKNOWLEDGMENTS

■ REFERENCES

(1) (a) Yaghi, O. M.; O'Keeffe, M.; Ockwig, N. W.; Chae, H. K.; Eddaoudi, M.; Kim, J. *Nature* **2003**, *423*, 705. (b) Li, H.; Eddaoudi, M.; O'Keeffe, M.; Yaghi, O. M. *Nature* **1999**, *402*, 276. (c) Rowsell, J. L. C.; Yaghi, O. M. *Microporous Mesoporous Mater.* **2004**, *73*, 3. (d) Stock, N.; Biswas, S. *Chem. Rev.* **2012**, *112*, 933.

(2) Zhou, H.-C.; Long, J. R.; Yaghi, O. M. *Chem. Rev.* **2012**, *112*, 673.

(3) (a) Kim, H.; Yang, S.; Rao, S. R.; Narayanan, S.; Kapustin, E. A.; Furukawa, H.; Umans, A. S.; Yaghi, O. M.; Wang, E. N. *Science* **2017**, *356*, 430. (b) Suh, M. P.; Park, H. J.; Prasad, T. K.; Lim, D.-W. *Chem. Rev.* **2012**, *112*, 782. (c) Bloch, E. D.; Queen, W. L.; Krishna, R.; Zadrozny, J. M.; Brown, C. M.; Long, J. R. *Science* **2012**, *335*, 1606.

(4) (a) Liu, J.; Chen, L.; Cui, H.; Zhang, J.; Zhang, L.; Su, C.-Y. *Chem. Soc. Rev.* **2014**, *43*, 6011. (b) Chughtai, A. H.; Ahmad, N.; Younus, H. A.; Laypkov, A.; Verpoort, F. *Chem. Soc. Rev.* **2015**, *44*, 6804. (c) Li, X.; Zhang, B.; Fang, Y.; Sun, W.; Qi, Z.; Pei, Y.; Qi, S.; Yuan, P.; Luan, X.; Goh, T. W.; Huang, W. *Chem. - Eur. J.* **2017**, *23*, 4266.

(5) (a) Chen, B.; Ockwig, N. W.; Millward, A. R.; Contreras, D. S.; Yaghi, O. M. *Angew. Chem.* **2005**, *117*, 4823. (b) Xiao, D. J.; Bloch, E. D.; Mason, J. A.; Queen, W. L.; Hudson, M. R.; Planas, N.; Borycz, J.; Dzubak, A. L.; Verma, P.; Lee, K.; Bonino, F.; Crocellà, V.; Yano, J.; Bordiga, S.; Truhlar, D. G.; Gagliardi, L.; Brown, C. M.; Long, J. R. *Nat. Chem.* **2014**, *6*, 590.

(6) (a) Li, X.; Guo, Z.; Xiao, C.; Goh, T. W.; Tesfagaber, D.; Huang, W. *ACS Catal.* **2014**, *4*, 3490. (b) Li, X.; Goh, T. W.; Li, L.; Xiao, C.; Guo, Z.; Zeng, X. C.; Huang, W. *ACS Catal.* **2016**, *6*, 3461. (c) Guo, Z.; Xiao, C.; Maligal-Ganesh, R. V.; Zhou, L.; Goh, T. W.; Li, X.; Tesfagaber, D.; Thiel, A.; Huang, W. *ACS Catal.* **2014**, *4*, 1340. (d) Metzger, E. D.; Brozek, C. K.; Comito, R. J.; Dincă, M. *ACS Cent. Sci.* **2016**, *2*, 148. (e) Majewski, M. B.; Howarth, A. J.; Li, P.; Wasielewski, M. R.; Hupp, J. T.; Farha, O. K. *CrystEngComm* **2017**, *19*, 4082.

(7) (a) He, N.-Y.; Woo, C.-S.; Kim, H.-G.; Lee, H.-I. *Appl. Catal., A* **2005**, *281*, 167. (b) Kuang, W.; Rives, A.; Fournier, M.; Hubaut, R. *Appl. Catal., A* **2003**, *250*, 221.

(8) (a) Musselwhite, N.; Na, K.; Sabyrov, K.; Alayoglu, S.; Somorjai, G. A. *J. Am. Chem. Soc.* **2015**, *137*, 10231. (b) Sabyrov, K.; Musselwhite, N.; Melaet, G.; Somorjai, G. A. *Catal. Sci. Technol.* **2017**, *7*, 1756.

(9) Djéga-Mariadassou, G.; Boudart, M. *J. Catal.* **2003**, *216*, 89.

(10) (a) Mastikhin, V. M.; Kulikov, S. M.; Nosov, A. V.; Kozhevnikov, I. V.; Mudrakovsky, I. L.; Timofeeva, M. N. *J. Mol. Catal.* **1990**, *60*, 65. (b) Ladera, R. M.; Ojeda, M.; Fierro, J. L. G.; Rojas, S. *Catal. Sci. Technol.* **2015**, *5*, 484.

(11) Jiang, J.; Yaghi, O. M. *Chem. Rev.* **2015**, *115*, 6966.

(12) Chen, J.; Thomas, J. M.; Sankar, G. *J. Chem. Soc., Faraday Trans.* **1994**, *90*, 3455.

(13) (a) Pelmenschikov, A. G.; Van Santen, R. A.; Janchen, J.; Meijer, E. *J. Phys. Chem.* **1993**, *97*, 11071. (b) Wichterlová, B.; Tvarůžková, Z.; Sobalík, Z.; Sarv, P. *Microporous Mesoporous Mater.* **1998**, *24*, 223. (c) Osmundsen, C. M.; Holm, M. S.; Dahl, S.; Taarning, E. *Proc. R. Soc. London, Ser. A* **2012**, *468*, 2000.

(14) Ravon, U.; Chaplais, G.; Chizallet, C.; Seyyedi, B.; Bonino, F.; Bordiga, S.; Bats, N.; Farrusseng, D. *ChemCatChem* **2010**, *2*, 1235.

(15) Thibault-Starzyk, F.; Travert, A.; Saussey, J.; Lavalley, J.-C. *Top. Catal.* **1998**, *6*, 111.

(16) Pinto, T.; Dufaud, V.; Lefebvre, F. *Appl. Catal., A* **2014**, *483*, 103.